Arch Appl Mech (2007) 77: 849–859
DOI 10.1007/s00419-007-0130-4

ORIGINAL

H. Dekker

Vibrational dynamics of modern lightrail modules

Received: 28 February 2006 / Accepted: 14 November 2006 / Published online: 30 March 2007

Abstract The vibrational frequency response of a modern lightrail module is considered in a simple model including dynamical features of the (typically aluminum) body with finite flexural rigidity, which inter alia reveals additional wheel–rail resonances. The model also allows to calculate the systems acoustic noise emission spectra, and to study the differences between aluminum and steel coaches.

1 Introduction

State-of-the-art trams are typically modular aluminium low-floor systems (e.g., [1,2]). The use of aluminium serves the purpose of weight—and, hence, energy consumption—reduction, also needed to compensate for weight-adding modern components such as computer systems and air conditioning, and the highly standardized modular design should reduce production costs. The last few years have shown a remarkable surge in the sales of fully low-floor trams. Since in this case the floor is in between the wheels, this concept has prompted the development of completely new trucks without the conventional wheel axis. In principle the low-floor wheel units cannot rotate horizontally, a clear disadvantage in, e.g., curves. Mainly for this reason, the vehicles have as small trucks as possible, which are placed almost rigidly under the center of relatively small modular units. In practice the novel truck design, in particular in its interaction with the aluminium body construction, has shown unconventional vibrational response, viz. resonances. Apart from leading to unstable wheel–rail contact (and increased polygonization of the wheels), this also causes enhanced noise production (e.g., [3]). In this article a simple mechanical model is studied for an interacting body–truck–wheel–rail system, which clarifies these fundamental design features from a theoretical physics point of view.

2 The model

Consider the mechanical system shown in Fig. 1. It consists (from bottom to top) of a wheel (with tyres) on an imperfect rail [specified as $\phi(t)$], a solid wheeltruck, and a flexible chassis body (with flexural rigidity coefficient γ, and length L). The various parts interact via linear springs (with Hooke constant C) and shock dampers (with Rayleigh coefficient D). The wheel mass is μ, the truck mass m, and the total static coach mass

H. Dekker
Private Institute for Advanced Study, Résidence Le Jardin Lijnbaansgracht 209L,
1016 XA Amsterdam, The Netherlands

H. Dekker (✉)
Institute for Theoretical Physics, University of Amsterdam, Valckenierstraat 65,
1018 XE Amsterdam, The Netherlands
E-mail: hadekk@science.uva.nl

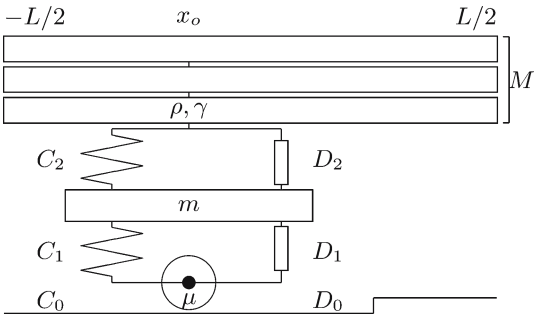

Fig. 1 Vibrational model of a lightrail unit, consisting of a nonrigid wheel (mass μ, internal spring and damping constants C_0, D_0), connected by external springs (C_1, C_2) and dampers (D_1, D_2) to a rigid truck (mass m) and a coach body (total mass M) consisting of flexible elastic plates (length L, effective mass density ρ, and stiffness parameter γ)

is M [i.e., the one-dimensional (1D) mass density $\varrho = M/L$]. The Lagrangian density for this system reads [4–7]

$$\mathcal{L} = L_o \delta(x - x_o) + \frac{1}{2}\varrho \left[\left(\frac{\partial y}{\partial t} \right)^2 - \gamma \left(\frac{\partial^2 y}{\partial x^2} \right)^2 \right], \tag{1}$$

with

$$L_o = \frac{1}{2}\mu\dot{\eta}^2 + \frac{1}{2}m\dot{y}_o^2 - \frac{1}{2}C_0\,(\eta - \phi)^2 - \frac{1}{2}C_1\,(\eta - y_o)^2 - \frac{1}{2}C_2\,(y_o - y(x_o))^2\,, \tag{2}$$

being the Lagrangian for wheel and truck (located at $x = x_o$, with $-L/2 < x_o < L/2$), while the dissipation function [4] is given by

$$\mathcal{F} = \frac{1}{2}D_0(\dot{\eta} - \dot{\phi})^2 + \frac{1}{2}D_1\,(\dot{\eta} - \dot{y}_o)^2 + \frac{1}{2}D_2\,(\dot{y}_o - \dot{y}(x_o))^2\,, \tag{3}$$

with $\phi(t)$ being the specified rail profile and where static gravitational effects (body bending and spring bias) have already been eliminated. The dynamics generated by Eqs. (1)–(3) can be written as

$$\frac{\partial^2 y}{\partial t^2} + \gamma \frac{\partial^4 y}{\partial x^4} = 0 \tag{4}$$

for the plate ($x \neq x_o, \pm L/2$),

$$D_2\,(\dot{y}(x_o) - \dot{y}_o) + C_2\,(y(x_o) - y_o) + \varrho\gamma \frac{\partial^3 y}{\partial x^3}\Big|_{x_o^-}^{x_o^+} = 0 \tag{5}$$

for the plate at $x = x_o$, and

$$m\ddot{y}_o + D_1\,(\dot{y}_o - \dot{\eta}) + D_2\,(\dot{y}_o - \dot{y}(x_o)) + C_1\,(y_o - \eta) + C_2\,(y_o - y(x_o)) = 0, \tag{6}$$

$$\mu\ddot{\eta} + D_0\left(\dot{\eta} - \dot{\phi}\right) + D_1\,(\dot{\eta} - \dot{y}_o) + C_0\,(\eta - \phi) + C_1\,(\eta - y_o) = 0 \tag{7}$$

for the wheel–truck unit. For the plate at $x = \pm\, L/2$ various boundary conditions are allowed [7]. Here the force-free edge conditions apply, viz.

$$\frac{\partial y}{\partial x}\Big|_{\pm L/2} = \frac{\partial^3 y}{\partial x^3}\Big|_{\pm L/2} = 0. \tag{8}$$

Equations. (4)–(8) uniquely specify the response of the system on the rail profile $\phi(t)$, i.e., on an external force $F(t) = C_0\phi(t) + D_0\dot{\phi}(t)$.

3 Rigid-body dynamics

3.1 Response functions

Consider the model of Sect. 2 in the rigid-body limit, viz. $\gamma \to \infty$. In that case, $y(x) \equiv y(x_o)$. Hence, integrating Eq. (4) along the plate, yields

$$\varrho\gamma \frac{\partial^3 y}{\partial x^3}\Big|_{x_o^-}^{x_o^+} \to M\ddot{y}(x_o), \tag{9}$$

so that Eq. (5) reduces to the equation of motion of the solid mass M. Setting

$$\eta = \frac{1}{2\pi}\int_{-\infty}^{\infty} \eta_\omega e^{i\omega t}\mathrm{d}\omega,\ \ y_o = \frac{1}{2\pi}\int_{-\infty}^{\infty} Y_\omega e^{i\omega t}\mathrm{d}\omega,\ \ y(x_o) = \frac{1}{2\pi}\int_{-\infty}^{\infty} y_\omega e^{i\omega t}\mathrm{d}\omega, \tag{10}$$

into Eqs. (5)–(6), one then obtains

$$\begin{aligned} -M\omega^2 y_\omega + (i\omega D_2 + C_2)(y_\omega - Y_\omega) &= 0,\\ -m\omega^2 Y_\omega + (i\omega D_1 + C_1)(Y_\omega - \eta_\omega) + (i\omega D_2 + C_2)(Y_\omega - y_\omega) &= 0, \end{aligned} \tag{11}$$

which allows one to compute the body and truck response to the wheel amplitude. For the truck response (with $\eta_\omega \equiv 1$) one finds

$$Y_\omega = (i\omega D_1 + C_1)(-M\omega^2 + i\omega D_2 + C_2)/Z_\omega, \tag{12}$$

where $Z_\omega = U_\omega + iV_\omega$ with

$$\begin{aligned} U_\omega &= C_1C_2 - (mC_2 + D_1D_2 + MC_{12})\,\omega^2 + Mm\,\omega^4,\\ V_\omega &= (C_1D_2 + C_2D_1)\,\omega - (mD_2 + MD_{12})\,\omega^3, \end{aligned} \tag{13}$$

where, e.g., $C_{12} = C_1 + C_2$. The body response reads

$$y_\omega = (i\omega D_1 + C_1)(i\omega D_2 + C_2)/Z_\omega. \tag{14}$$

Finally, using Eqs. (7) and (12), the wheel response can be written as

$$\eta_\omega = F_\omega/\left[C_0 + i\omega D_0 + (C_1 + i\omega D_1)(1 - Y_\omega) - \mu\omega^2\right], \tag{15}$$

where $F_\omega = (C_0 + i\omega D_0)\phi_\omega$. Note that $\eta_{\omega\to\infty} = -F_{\omega\to\infty}/(\mu\omega^2)$. On the other hand, since $Y_{\omega\to 0} = 1 + (m + M)\,\omega^2/C_1$, one has $\eta_{\omega\to 0} = -F_{\omega\to 0}/(C_0 + i\omega D_0 - M_o\omega^2)$ with $M_o = \mu + m + M$, e.g., with $D_0 = 0$, the wheel response on a unit step in the rail profile follows from $F_\omega = -i(\pi/2\omega)C_0$.

3.2 Basic parameters

Both truck and body resonances follow from $Z_\omega = 0$. With $M \gg m$, the body resonance frequency typically obeys $\omega_2 \ll (C_1/m)^{1/2}$. In that case one obtains $Z_\omega/C_{12} \approx (C_1C_2)/C_{12} + i\omega D_2 - M\omega^2$, so that $\omega_2 \approx (C_1C_2/MC_{12})^{1/2}$. In practice $C_2 \ll C_1$, hence $\omega_2 \approx (C_2/M)^{1/2}$. For the truck resonance one has $\omega_1 \gg \omega_2$ and $Z_\omega/M\omega^2 \approx -(C_{12} + i\omega D_{12} - m\omega^2)$, so that $\omega_1 \approx (C_{12}/m)^{1/2} \approx (C_1/m)^{1/2}$. Finally, with $m \gg \mu$, at the wheel resonance $\omega_0 \gg \omega_1$ one has $Y_\omega \ll 1$, so that Eq. (15) yields $\omega_0 \approx (C_{01}/\mu)^{1/2}$.

The damping must be set at its critical value, viz. neither strong nor weak. Too little is uncomfortable for the passengers (swaying ride), and gives rise to large forces in the construction near resonance. On the other hand, too much is uncomfortable as well (bumpy ride), and moreover leads to increasing forces at higher frequencies. For example, for the body the effective friction coefficient approximately equals D_2/M, and critical damping amounts to $D_2/2M \approx \omega_2$. The truck is critically damped if $D_{12}/2m \approx \omega_1$, and for the wheel one should take $D_{01}/2\mu \approx \omega_0$. The rigorous three-body analysis is given in the Appendix.

The total mass of a five-module lightrail tram typically amounts to $M_{\mathrm{tot}} \approx 35$ ton when empty and $M_{\mathrm{tot}} \approx 55$ ton when fully loaded, and has three trucks (two of which are traction units with two electric motors each, and one of which is free running) with four wheels each. The mass of a wheel is approximately $\mu \approx 80$ kg.

The mass of a traction truck is about 1,600 kg, i.e., $m_{\rm tr} \approx 400\,{\rm kg}$ per wheel, while that of the free-running truck is roughly half that value, i.e., $m_{\rm fr} \approx 2,00\,{\rm kg}$ per wheel. Consequently, in our model the body mass (for a half-filled module) is taken to be $M = (M_{\rm tot} - m_{\rm fr} - 2m_{\rm tr} - 12\mu)/20$ per wheel, i.e., $M \approx 2,000\,{\rm kg}$.

The value of the secondary spring constant C_2 is basically set by practical constraints on both the body resonance frequency and the static gravitational bias. The latter amounts to $y_{\rm b} = Mg/C_2$. With, e.g., $C_2 = 4\times10^5{\rm kg\,s^{-2}}$ one obtains $y_{\rm b} \approx 5\,{\rm cm}$ and $\omega_2 \approx 14\,{\rm s^{-1}}$ (i.e., about 2 Hz). The ensuing approximate value for the secondary damper is $D_2 \approx 5.6\times10^4\,{\rm kg\,s^{-1}}$. The secondary suspension typically consists of a helical compression spring.

The primary suspension is usually made of rubber. An elastic cylinder of length ℓ and radius r yields a spring constant of $C = E\pi r^2/\ell$, where $E \approx 30\times10^6\,{\rm N\,m^{-2}}$ is the Young's modulus for rubber (see, e.g., [10]). With $r \approx \ell \approx 10\,{\rm cm}$, this gives $C_1 \approx 10^7\,{\rm kg\,s^{-2}}$ which implies a proper static bias within the wheel-truck unit of a few millimeter, and a traction truck resonance at $\omega_1 \approx 160\,{\rm s^{-1}}$ (i.e., about 25 Hz). For the primary damper one may write $D_1 \approx (1/\xi - 1)D_2$, where $\xi = (MC_2/mC_1)^{1/2}$. Clearly, $D_1 > 0$ requires $\xi < 1$ (see the Appendix). Since the vehicle has twice as many traction trucks as free running ones, the primary suspension is designed using $m_{\rm tr}$. In that case $\xi \approx 1/\sqrt{5}$, so that $D_1 \approx 6.9\times10^4\,{\rm kg\,s^{-1}}$.

A wheel may be shock absorbing using rubber tyres. With thickness $\ell \approx 1\,{\rm cm}$, and an effective transverse area of some $\mathcal{A} \approx 5\times10\,{\rm cm^2}$, using $C = E\mathcal{A}/\ell$ yields $C_0 \approx 1.5\times10^7\,{\rm kg\,s^{-2}}$. The wheel resonance frequency then becomes $\omega_0 \approx 430\,{\rm s^{-1}}$ (i.e., about 70 Hz). Writing $D_0 \approx (1/\xi_o - 1)D_1$ where $\xi_o = (1-\xi)\nu$ with $\nu = (mC_1/\mu C_0)^{1/2}$, and using the above value for ξ, one finds $1/\xi_o \approx 0.99$ so that $D_0 \ll D_1$. In fact, the internal damping of rubber is very small, viz. of the order of $D \approx 10^3\ell$, i.e., $D_0 \approx 10\,{\rm kg\,s^{-1}}$. So, $D_0 \approx 0$.

4 General spectra

4.1 The body mass M_ω

The general solution of Eq. (4) with the boundary conditions (8) may be written as in Eq. (10) with

$$\begin{aligned} y_\omega(x < x_o) &= a_{\rm l}\cos\varphi_{\rm l} + b_{\rm l}\cosh\varphi_{\rm l},\\ y_\omega(x > x_o) &= a_{\rm r}\cos\varphi_{\rm r} + b_{\rm r}\cosh\varphi_{\rm r}, \end{aligned} \tag{16}$$

where $\varphi_{\rm l} = k(x+L/2)$, $\varphi_{\rm r} = k(x-L/2)$, with $k = \gamma^{-1/4}|\omega|^{1/2}$. Note that this implies a frequency-dependent (group) velocity $v_{\rm g} = 2\gamma^{1/4}|\omega|^{1/2}$. Continuity of $y(x)$, $\partial y/\partial x$, and $\partial^2 y/\partial x^2$ at $x = x_o$ yields

$$a_{\rm r} = a_{\rm l}\frac{\cos\varphi_{\rm lo}}{\cos\varphi_{\rm ro}}, \quad b_{\rm r} = b_{\rm l}\frac{\cosh\varphi_{\rm lo}}{\cosh\varphi_{\rm ro}}, \quad b_{\rm l} = a_{\rm l}\frac{\cosh\varphi_{\rm ro}}{\cos\varphi_{\rm ro}}\,\frac{\sin kL}{\sinh kL}, \tag{17}$$

with, e.g., $\varphi_{\rm ro} = \varphi_{\rm r}(x_o)$. Using Eq. (17) in Eq. (16), one obtains

$$y_\omega(x_o) = 2a_{\rm l}f_o\cos\varphi_{\rm lo}, \quad \frac{\partial^3 y_\omega}{\partial x^3}\Big|_{x_o^-}^{x_o^+} = -2a_{\rm l}k^3\frac{\sin kL}{\cos\varphi_{\rm ro}}, \tag{18}$$

where

$$f_o = \frac{1}{2}\left(1 + \frac{\cosh\varphi_{\rm lo}}{\cos\varphi_{\rm lo}}\,\frac{\cosh\varphi_{\rm ro}}{\cos\varphi_{\rm ro}}\,\frac{\sin kL}{\sinh kL}\right). \tag{19}$$

Now defining a frequency-dependent effective mass M_ω, in line with Eq. (9) and using Eq. (18), as

$$M_\omega = \frac{M}{f_o\cos\varphi_{\rm lo}\cos\varphi_{\rm ro}}\,\frac{\sin kL}{kL}, \tag{20}$$

(where use was made of $\gamma k^4/\omega^2 = 1$ and $\varrho L = M$) the response formulae of Sect. 3 carry over to the general case, with M being replaced by M_ω. Note that $M_{\omega\to0} = M$.

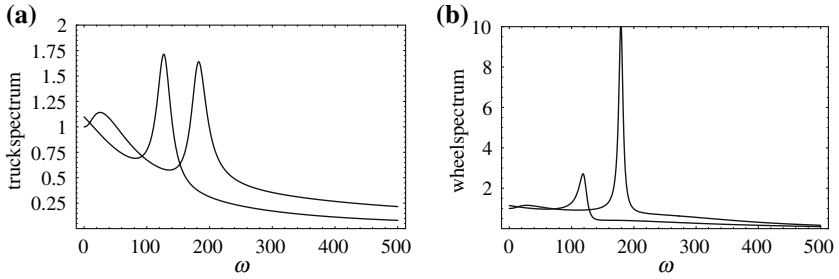

Fig. 2 Vibrational spectra for **a** truck and **b** wheel [*Left curves*: traction module (shifted to the left over $50\,\mathrm{s}^{-1}$); *right curves* free-running units], showing fundamental flexural body resonance and free-running truck enhancement for the wheel. See text below for system parameter values

4.2 Flexural rigidity

With $M_\omega \in (-\infty, \infty)$, the spectra (e.g., [8])

$$S_\mathrm{W}(\omega) = \eta_\omega \eta_{-\omega},\ S_\mathrm{T}(\omega) = Y_\omega Y_{-\omega},\ S_\mathrm{B}(\omega) = y_\omega y_{-\omega} \tag{21}$$

for the wheel (with $\phi_\omega = 1$), truck (with $\eta_\omega = 1$), and body (at x_o) become intricate, e.g., with $C_2 \ll C_1$ one may write

$$Y_\omega \approx (C_1 + i\omega D_1)/(C_1 + i\omega D_{1\omega} - m_\omega \omega^2), \tag{22}$$

with $D_{1\omega} = D_1 + D_\omega$, $D_\omega = D_2/[1+(D_2/\omega M_\omega)^2]$, $m_\omega = m + M_\omega/[1+(\omega M_\omega/D_2)^2]$. Clearly, the spectrum $S_\mathrm{T}(\omega)$ will have a local maximum when D_ω drops from its normal rigid-body value D_2 to zero, i.e., at some $\omega_\gamma = \gamma^{1/2}(2\pi n/L)^2\ M_{\omega_\gamma} = 0\ (n = 1, 2, \cdots)$. Using Eq. (20), one finds $M_\omega \approx 2M(\omega^{1/2} - \omega_\gamma{}^{1/2})/\omega_\gamma{}^{1/2}$, so that the frequency interval set by $M_\omega \approx D_2/\omega_\gamma$ amounts to $\delta\omega_\gamma \approx D_2/2M$, which equals the body frequency $\omega_2 \approx 2\,\mathrm{Hz}$. That is, $\delta\omega_\gamma \ll \omega_\gamma$. If $\omega_\gamma \approx \omega_1$, the spectral density $S_\mathrm{T} \approx (C_1 + \omega^2 D_1)/(\omega D_{1\omega})^2$ is thus found to increase by a factor $(D_{12}/D_1)^2$ (≈ 4) over the small frequency interval $\delta\omega_\gamma$. A similar effect exists, of course, for the body and $S_\mathrm{B}(\omega \approx \omega_1)$ is easily shown to be enhanced by a factor M/m_tr (≈ 5) at $\omega \approx \omega_\gamma$.

Substituting Eq. (22) into Eq. (15) for the wheel (at $\omega \approx \omega_1$, and with $D_0 = 0,\ \phi_\omega = 1$), one finds

$$\eta_\omega \approx C_0/(C_{0\omega} + i\,D_{0\omega} - \mu_\omega \omega^2), \tag{23}$$

where $C_{0\omega} = C_0 + (D_\omega/D_{1\omega})C_1$, $D_{0\omega} = (D_1/D_{1\omega})D_\omega + (C_1/D_{1\omega})m_\omega\,\omega$, and $\mu_\omega = \mu + (D_1/D_{1\omega})m$. In the rigid-body case (i.e., $D_\omega = D_2$) the ensuing spectrum $S_\mathrm{W}(\omega)$ would have a resonance at $\omega \approx ([C_0 + (D_2/D_{12})C_1]/[\mu + (D_1/D_{12})m])^{1/2}$. With $m \gg \mu$ (see Sect. 3.2) this can be rewritten as $\omega \approx (\omega_0\omega_1)^{1/2} \gg \omega_1$, so that $S_\mathrm{W}(\omega_1) \approx 1$. On the other hand, if $D_\omega = 0$, this resonance frequency shifts downward to $\omega \approx C_0/(\mu + m) \approx \omega_1$; one then gets $S_\mathrm{W} \approx (C_0 D_1/m\omega_\gamma C_1)^2$. Note the inverse square dependence on m and ω_γ. The enhancement may be rewritten as $4(C_0/C_1)^2(D_1/D_{12})^2\ (\omega_1/\omega_\gamma)^2(m_\mathrm{tr}/m)^2 \approx 2(m_\mathrm{tr}/m)^2$, which amounts to an unfavorable extra factor of four for the free-running truck. Finally, notice that for $\omega_\gamma \approx \omega_0 \gg \omega_1$ one has $Y_\omega \approx (C_1 - i\omega D_1)/m\omega^2$, which is independent of D_ω so that both wheel and truck become independent of the flexural body resonances at frequencies well above the truck resonance.

The flexural rigidity coefficient γ in Eq. (1) is given by $\gamma = \frac{1}{12}(E/\overline{\rho})d^2/(1-\sigma^2)$, where [7] E is the Young's modulus, $\overline{\rho} = \alpha\rho_\mathrm{b}$ is the effective mass per unit volume (with ρ_b being the solid bulk density, and α the filling factor), σ is the Poisson ratio, and d is the plate thickness. In practice, $0 < \sigma < 1/2$. With $\sigma \ll 1$ for metals, one has [7] $c_\parallel \approx [E/\rho_\mathrm{b}(1-\sigma^2)]^{1/2}$ for the velocity of propagation of longitudinal acoustic waves in an infinite medium. Hence, $\gamma^{1/2} \approx c_\parallel d/(12\alpha)^{1/2}$. Consequently, $k = (12\alpha)^{1/4}(\omega/c_\parallel d)^{1/2}$. This dispersion relation holds for all $kd \ll 1$. Numerically, $c_\parallel \approx 6\times10^3\ \mathrm{m\ s}^{-1}$ for both aluminium and steel. For aluminium sandwich constructions one has, e.g., $\alpha \approx 1/10$ and $d \approx 3\,\mathrm{cm}$, viz. $\gamma^{1/2} \approx 164\,\mathrm{m}^2\ \mathrm{s}^{-1}$. Taking $L = 6$ m (one-fifth of the typical vehicle length), one then obtains $\omega_\gamma \approx 180\ \mathrm{s}^{-1}$, i.e., about 28 Hz for the fundamental flexural body resonance, which may thus indeed be close to the truck resonance $\omega_1 \approx 25$ resp. 35 Hz (traction resp. free-running).

All formula are easy to compute using Mathematica 5. Figure 2a shows the truck spectrum $S_\mathrm{T}(\omega)$ with $\eta_\omega = 1$, using Eq. (12) [and M replaced by M_ω according to Eq. (20)] with $M = 2,000\,\mathrm{kg}$, $\mu = 80\,\mathrm{kg}$, $L = 6\,\mathrm{m}$, and $C_0 = 1.2\times10^7$, $C_1 = 10^7$, $C_2 = 4\times10^5\,\mathrm{kg\ s}^{-2}$ (see Sect. 3.2); the dampers are set at their

exact critical values (see Appendix) $D_0 = 0$, $D_1 = 6.4\times10^4$, $D_2 = 5.4\times10^4\,\mathrm{kg\ s^{-1}}$. The spectra pertain (from left to right) to the traction respectively free-running truck (with $m_{\mathrm{tr}} = 400$ and $m_{\mathrm{fr}} = 200\,\mathrm{kg}$) for an aluminium coach with $\gamma^{1/2} = 164\,\mathrm{m^2\ s^{-1}}$ (see above), with the former for clarity being shifted to the left over $50\,\mathrm{s^{-1}}$. Figure 2b is similar, but for the wheel spectrum $S_{\mathrm{W}}(\omega)$ with $\phi_\omega = 1$. The extra enhancement factor $(m_{\mathrm{tr}}/m_{\mathrm{fr}})^2 \approx 4$ for the free-running wheel has been discussed above. Further, with these parameters one has $S_{\mathrm{B}} \approx S_{\mathrm{T}}$. Throughout, $x_o = 0$.

4.3 Dynamic stability

While at high speed a wheel running on a bumpy surface—a nonholonomic mechanical problem [4]—will eventually always fly off due to centrifugal effects, intrinsic system resonances as found in the preceding section may be a potential hazard at considerably lower speeds. Let us therefore investigate in our model the dynamic stability of the wheel on the rail.

Let the rail profile (amplitude in the y-direction) be given by $\phi(t) = \phi_o\cos\kappa x$, where $x = U_o t$ with constant vehicle velocity $\dot{x} = U_o$. The total force between the wheel and rail consists of two components, a force $F_\parallel(t)$ parallel to the surface and a force $F_\perp(t)$ perpendicular to it. The former takes care of the traction (to keep the vehicle at the constant speed U_o), while the latter determines the stability of the wheel–rail contact. In particular, if $F_\perp(t_o) > 0$ at some t_o the wheel will lift off at $t = t_o + 0$. For the traction truck the actual motor force F_{tr} is parallel to the surface, i.e., it has no normal component and need not be determined in detail. Hence, $F_\perp = (F_{\mathrm{w}} + F_{\mathrm{g}})\cos\theta$ where $F_{\mathrm{w}} = C_0(\eta - \phi) + D_0(\dot{\eta} - \dot{\phi})$ is the instantaneous dynamic force between the wheel and rail, $F_{\mathrm{g}} = -M_o g$ (with $M_o = \mu + m + M$) and $\theta = \arctan(\mathrm{d}\phi/\mathrm{d}x)$ (with $\mathrm{d}\phi/\mathrm{d}x = \dot{\phi}/U_o$).

On the other hand, the free-running module is kept at the constant speed $\dot{x} = U_o$ through the pulling (or pushing) of the traction modules. Hence, the externally applied motor force F_{fr} lies along the x-axis and, therefore, does have a component $F_{\mathrm{fr}}\sin\theta$ normal to the surface. To determine F_{fr}, note that due to the constraint [4] of the motion (up to t_o), the only dynamic part of the motor force is its component $F_{\mathrm{fr}}\cos\theta$ tangential to the surface, which implies an effective driving force $F_{\mathrm{fr}}\cos^2\theta$ in the horizontal x-direction. Similarly, the constraint also leads to an effective horizontal driving force $(F_{\mathrm{w}} + F_{\mathrm{g}})\sin\theta\cos\theta$ due to the module's vibrations. To maintain free-running at a constant speed, the total dynamic force in the x-direction should be zero, which yields $F_{\mathrm{fr}} = -(F_{\mathrm{w}} + F_{\mathrm{g}})\tan\theta$. Consequently, in this case one finds $F_\perp = (F_{\mathrm{w}} + F_{\mathrm{g}})\sec\theta$. Note that the free-running module is potentially more violently unstable than the traction unit. In what follows, however, only small $\theta \ll 1$ (i.e., $\kappa\phi_o \ll 1$) will be considered so that $F_\perp = F_{\mathrm{w}} + F_{\mathrm{g}}$ for both cases.

Given $\phi(t)$, the dynamical contact force now becomes

$$F_\perp(t) = A_\omega\cos\omega t + B_\omega\sin\omega t - M_o g, \tag{24}$$

with

$$\begin{aligned} A_\omega &= -C_0\phi_o(1 - \mathrm{Re}\,\eta_\omega) - \omega D_0\phi_o\,\mathrm{Im}\,\eta_\omega, \\ B_\omega &= -C_0\phi_o\,\mathrm{Im}\,\eta_\omega + \omega D_0\phi_o(1 - \mathrm{Re}\,\eta_\omega), \end{aligned} \tag{25}$$

where η_ω is given in Eq. (15), and $\omega = \kappa U_o$. It is worth noting that Eq. (25) leads to a finite limit for $C_0 \to \infty$. Namely, from Eq. (7) one obtains $\eta \approx \phi + \eta^{(1)}/C_0 + \mathcal{O}(1/C_0^2)$ with $\eta^{(1)} = C_1(\phi - y_o) + D_1(\dot{\eta} - \dot{y}_o) - \mu\omega^2$. This yields $F_{\mathrm{W}} \approx \eta^{(1)}$, which represents the vibrational force of the truck supplemented with the centrifugal force of the wheel. The limiting expressions for A_ω and B_ω are obtained from Eq. (25) by replacing (C_0, D_0) by (C_1, D_1) and η_ω by Y_ω, and adding the centrifugal term $-\mu\omega^2\phi_o$ to A_ω.

The force $F_\perp(t)$ in Eq. (24) has extrema at $t = \omega^{-1}\mathrm{arccot}(\omega A_\omega/B_\omega)$ and its maximum value amounts to

$$F_{\max}(\omega) = \sqrt{A_\omega^2 + B_\omega^2} - M_o g, \tag{26}$$

which is shown in Fig. 3 (for the same parameter sets as in Fig. 2, and $\phi_o = 1\,\mathrm{mm}$). For clarity the plot for the traction module is again shifted to the left over $50\,\mathrm{s^{-1}}$. At $\omega = 0$ the wheel is pushed firmly on the rails by the static force $F_{\max} = -M_o g$, while at frequencies well beyond $\omega_{\mathrm{c}} = \sqrt{M_o g/\mu\phi_o}$ ($\omega_{\mathrm{c}} \approx 10^3\,\mathrm{s^{-1}}$) centrifugal fly off may set in. Evidently, while the traction wheel is stable for all practically relevant frequencies, the wheel–rail contact for the free-running wheel is unstable near $\omega_\gamma \approx 180\,\mathrm{s^{-1}}$ (see, e.g., [3]). At moderate city speeds of the order of $U_o \approx 6\,\mathrm{m\ s^{-1}}$ (i.e., about $22\,\mathrm{km\ h^{-1}}$) this corresponds to a wavelength $\lambda \approx 20\,\mathrm{cm}$, which agrees with recently observed novel wavy rail distortions (see, e.g., http:www.baluw.nl/combino). On a wheel with a diameter of 60 cm this would amount to a hexagonal deformation (i.e., a ten-sided polygon).

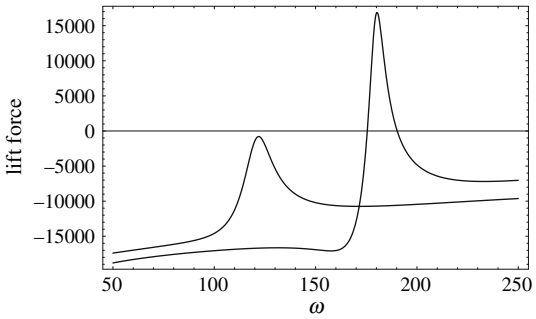

Fig. 3 Lift force for wheel–rail contact, following Eq. (26), for both traction (*left curve* displaced over $50\,\mathrm{s}^{-1}$) and free-running wheel (*right*) of an aluminium lightrail module. The system parameters are identical to those for Fig. 2

5 Acoustics

5.1 Noise spectra

Imperfect wheel–rail contact produces polygonization (and, hence, wear and high maintenance costs) of the wheel, and a specific wave-type rail damage. This also leads to enhanced noise emission levels. The physiology of sound perception is a complicated subject, but a sensible impression of the acoustic characteristics of the vehicle may be obtained on the basis of the mechanical spectra as follows. First of all, the acoustic spectrum $S_\mathrm{a}(\omega)$ must be calculated by smoothing the mechanical spectrum $S_\mathrm{m}(\omega)$ using a terts—i.e. a major third (see, e.g., [9])—filter $P(x)$. In addition, since the human ear only processes frequencies above $f_\ell \approx 20\,\mathrm{Hz}$, both input and output of the smoothing process involve a low-pass filter $Q(\omega)$. The results are practically independent of the specifics of the filter functions, and the acoustic spectra are conveniently computed as

$$S_\mathrm{a}(\omega) = Q(\omega) \int_1^\infty P(x)\, Q(x\,\omega) S_\mathrm{m}[x\,\omega/(1+w)]\mathrm{d}x, \tag{27}$$

with

$$P(x) = \frac{(x-1)}{w^2} \exp\left[-\frac{1}{2}\left(\frac{x-1}{w}\right)^2\right], \tag{28}$$

where $w = 2^{2/7} - 1$ for the temperate musical scale (or $w = 1/4$ for the absolute scale), and with

$$Q(\omega) = \exp[-(\omega_\ell/\omega)^2], \tag{29}$$

where $\omega_\ell = 40\pi\ \mathrm{s}^{-1}$.

The acoustic truck spectrum (with $\phi_\omega = 1$) corresponding to the vibrational spectra of Fig. 2 is shown in Fig. 4a, which is obtained by applying Eq. (27) to the mechanical spectrum $S_\mathrm{TW} = S_\mathrm{T} S_\mathrm{W}$. As before, the left curve applies to the traction module, while the right one pertains to the free-running case. Figure 4b shows the same spectrum for a welded steel module, which is typically of the monocoque type. In that case, the effective flexural rigidity in Eq. (1) can be estimated by applying the theory of elasticity (see [7]) to a hollow tube with Young's modulus E, filled by a medium of practically zero mass density but with modulus E_o. For a duct with rectangular cross section (of infinite width) and $E_o = E$, one recovers the result of Sect. 4.2 for a sandwich construction. However, for a similar tubular element (with infinitesimal wall thickness) with $E_o = 0$ one obtains $\gamma^{1/2} \approx c_\parallel d/2$. With, e.g., $d = 15\,\mathrm{cm}$ this yields $\gamma^{1/2} = 450\,\mathrm{m}^2\ \mathrm{s}^{-1}$. In fact, the spectra in Fig. 4b are already practically indistinguishable from the perfectly rigid case (the transition takes place around $\gamma^{1/2} \approx 300\,\mathrm{m}^2\ \mathrm{s}^{-1}$).

Figure 4 shows that the sound production by the trucks of aluminium coaches tends to be enhanced in comparison with steel ones, in particular in the low but audible frequency range of 20–50 Hz ($\omega \approx 200\,\mathrm{s}^{-1}$). This feature may now be understood to have the same dynamical origin as the wheel's tendency to polygonize (and rumble on self-produced wave-type rail distortions). It is worth remarking that the lightrail body itself does not emit sound waves at frequencies below $\omega_\mathrm{e} = \gamma^{-1/2} c_\mathrm{a}^2$, but merely drags an exponentially decaying surface wave along. Note that $\omega_\mathrm{e} \approx 720\,\mathrm{s}^{-1}$ (i.e., 115 Hz) for $\gamma^{1/2} = 164\,\mathrm{m}^2\ \mathrm{s}^{-1}$, respectively $\omega_\mathrm{e} \approx 260\,\mathrm{s}^{-1}$ (i.e., 42 Hz) for $\gamma^{1/2} = 450\,\mathrm{m}^2\ \mathrm{s}^{-1}$

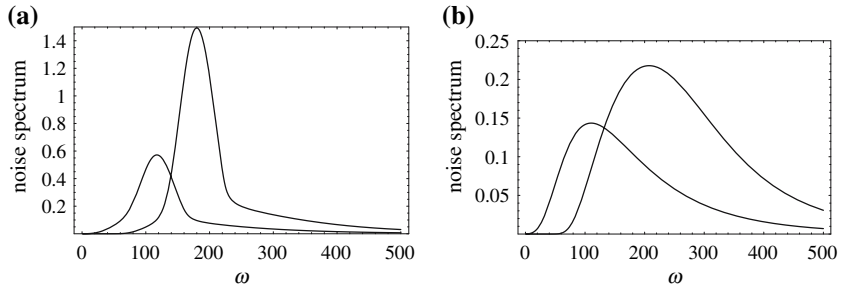

Fig. 4 Terts-averaged acoustic spectra for **a** aluminium [flexural rigidity $\gamma^{1/2} = 164\,\mathrm{m}^2\,\mathrm{s}^{-1}$] and **b** steel [$\gamma^{1/2} = 450\,\mathrm{m}^2\,\mathrm{s}^{-1}$] body, both for traction (*left curve*, displaced over $50\,\mathrm{s}^{-1}$) and free-running truck (*right curve*). System parameters other than γ are identical to those for Figs. 2 and 3

5.2 Loudness levels

Let us estimate the order of magnitude of the loudness. Strictly speaking, this is a rather difficult subject since the observed power *inter alia* depends on the frequency (i.e., on the wavelength $\lambda_\mathrm{a} = 2\pi c_\mathrm{a}/\omega$ in air), on the dimensions ℓ and shape of (and distance r to) the source, as well as on the (frequency and sound-level dependent) properties of the human ear (e.g., [11]). Nevertheless, some general conclusions can be drawn if $r \gg \ell$. In that case, the total energy emitted per unit of time by a source with surface area Ω may be given in the dipole approximation as [12]

$$I(\omega) = \rho_\mathrm{a} c_\mathrm{a} \overline{\mathbf{u}^2} \Omega \mathsf{F}(k_\mathrm{a}\ell), \tag{30}$$

with $k_\mathrm{a} = \omega/c_\mathrm{a}$, where $\mathsf{F}(z) \approx z^4/(64 + z^4)$, and $\mathbf{u}$ is the normal velocity at the source surface. Further, $\rho_\mathrm{a} = 1.2\,\mathrm{kg\ m}^{-3}$ and $c_\mathrm{a} = 344\,\mathrm{m\ s}^{-1}$. The energy flux on a (half-)sphere of radius r is given by $\Phi(\omega) = I(\omega)/2\pi r^2$.

As in Sect. 4.3, let the rail profile amplitude be ϕ_o so that $\overline{\mathbf{u}^2} = \frac{1}{2}\omega^2 S_\mathrm{a}(\omega)\phi_o^2$. For a truck the vibrating surface area amounts to $\Omega \approx 2\ell^2$, with $\ell \approx 2$ m. At the spectral peak near $\omega_\mathrm{m} \approx 200\,\mathrm{s}^{-1}$ (i.e.,$k_\mathrm{a} \approx 0.58\,\mathrm{m}^{-1}$, $\lambda_\mathrm{a} \approx 10.8\,\mathrm{m}$) one then has $k_\mathrm{a}\ell \approx 1.16$, so that $I(\omega_\mathrm{m}) \approx 6.6\times10^7 S_\mathrm{a}(\omega_\mathrm{m})\,\phi_o^2\,\mathsf{F}(1.16)\,\mathrm{Js}^{-1}$. With $\phi_o = 1\,\mathrm{mm}$ and $\mathsf{F}(1.16) \approx 2.8\times10^{-2}$, the energy flux at the (ISO) standard distance of $r = 7.5$ m from the source then yields $\Phi(\omega_\mathrm{m}) \approx 5.2\times10^{-3} S_\mathrm{a}(\omega_\mathrm{m})\,\mathrm{Wm}^{-2}$. Using Fig. 4 one thus arrives at $\Phi(\omega_\mathrm{m}) \approx 3.1\times10^{-3}$, respectively $7.8\times10^{-3}\,\mathrm{Wm}^{-2}$ for the aluminium traction and free-running case, and $\Phi(\omega_\mathrm{m}) \approx 7.3\times10^{-4}\ 1.1\times10^{-3}\,\mathrm{Wm}^{-2}$ for the corresponding steel ones.

Loudness level (measured in phon) is defined as

$$\mathsf{L}(\omega) = \mathsf{d}(\omega)\log\left[\Phi(\omega)/\Phi_o(\omega)\right]. \tag{31}$$

At $\omega = 2\pi f_\mathrm{r}$ with $f_\mathrm{r} = 10^3\,\mathrm{Hz}$ the hearing threshold amounts to $\Phi_o = 10^{-12}\,\mathrm{Wm}^{-2}$, and with $\mathsf{d}(\omega_\mathrm{r}) = 10$ the loudness level is given in decibels (dB). However, from the standard equal-loudness-level contours (see, e.g., [13,14]) one infers that for $\omega < 2\pi f_\mathrm{s}$ with $f_\mathrm{s} \approx 10^{14/5} \approx 630\,\mathrm{Hz}$ the threshold approximately scales as $\Phi_o(\omega) \approx (\omega/\omega_\mathrm{s})^{-\varepsilon}\times10^{-12}\mathrm{Wm}^{-2}$, with $\varepsilon = 5$. Therefore, at $\omega_\mathrm{m} = 200\,\mathrm{s}^{-1}$ (i.e., 31.8 Hz) one has $\Phi_o(\omega_\mathrm{m}) \approx 3\times10^{-6}\mathrm{Wm}^{-2}$. In addition, since all loudness levels $\mathsf{L} > 0$ scale approximately similarly [but having exponents $\varepsilon(\mathsf{L}) < 5$, with $d\varepsilon/d\mathsf{L} \approx 0.05$], the coefficient d is found to vary with the frequency as $\mathsf{d}(\omega) \approx 20/\log(\omega/\omega_\mathrm{d})$, where $\omega_\mathrm{d} = 0.01\,\omega_\mathrm{s}$. This yields $\mathsf{d}(\omega_\mathrm{m}) \approx 28.5$ at $\omega_\mathrm{m} = 31.8\,\mathrm{Hz}$. Using the above energy flux values in $\mathsf{L}(\omega_\mathrm{m}) \approx 28.5\log(10^6\Phi/3)$ one thus arrives at $\mathsf{L}_\mathrm{tr} \approx 84.5$ resp. $L_\mathrm{fr} \approx 96.9\,\mathrm{dB}$ for the aluminium, and $\mathsf{L}_\mathrm{tr} \approx 67.6$ resp. $L_\mathrm{fr} \approx 73.2\,\mathrm{dB}$ for the steel cases.

While these results are in line with the L values found in practice (see, e.g., http:www.baluw.nl/combino), it should once more be remarked that absolute sound levels are theoretically less substantiated than differences, where in, e.g., the relatively strong dependence on ϕ_o, ω and ℓ [note that $\Phi(\omega_\mathrm{m}) \sim \phi_o^2\omega^6\ell^6$], which is enhanced by the large value of $\mathsf{d}(\omega_\mathrm{m})$, drops out in $\Delta\mathsf{L} = \mathsf{L}_\mathrm{fr} - \mathsf{L}_\mathrm{tr}$. Note then that $\Delta\mathsf{L} \approx 12.4\,\mathrm{dB}$ for aluminium, while $\Delta\mathsf{L} \approx 5.6\,\mathrm{dB}$ for steel modules. Computing the loudness level $\mathsf{L}(\omega)$ shows that the exact values are somewhat bigger, mainly because the traction and free-running trucks have slightly different ω_m. One finds $\Delta\mathsf{L} \approx 18.5$ and $\Delta\mathsf{L} \approx 10.5\,\mathrm{dB}$, respectively.

These numbers do not noticeably change upon including the noise from the wheels and the body. Namely, as already mentioned above Fig. 4, the nonrigid body emits sound waves only for frequencies $\omega_\mathrm{e} > \gamma^{-1/2}c_\mathrm{a}^2$,

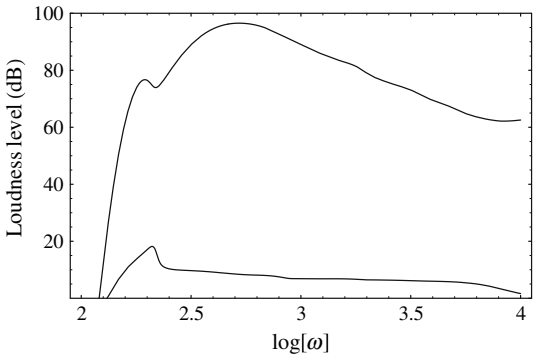

Fig. 5 Loudness levels of module with flexural rigidity $\gamma^{1/2} = 164\,\mathrm{m}^2\,\mathrm{s}^{-1}$ in decibels, as a function of ${}^{10}\log\omega$. The *upper curve* represents L_{tot} for the traction unit. The *lower curve* gives the difference in loudness level between the free-running unit and the traction one. System parameters are identical to those for Figs. 2, 3, 4

and presently $\omega_{\mathrm{e}} > \omega_{\mathrm{m}}$. Above ω_{m}, the body's noise intensity can be calculated using Eq. (30) with $\Omega \approx \ell L$ and c_{a} being replaced by (e.g., [15]) the group velocity $v_{\mathrm{a}} = 1/[dk_{\mathrm{a}}(\omega)/d\omega]$, where $k_{\mathrm{a}}(\omega) = (c/\omega)[1 - (c_{\mathrm{a}}k(\omega)/\omega)^2]^{1/2}$ (with $k(\omega) = \gamma^{-1/4}|\omega|^{1/2}$ being the body's wave number). In addition, $k_{\mathrm{a}}(\omega)$ replaces $k_{\mathrm{a}} = \omega/c_{\mathrm{a}}$ in F. The ensuing body loudness level typically rises fairly steeply to a peak value of the order of 80 dB somewhat above ω_{e}, and from thereon decreases—in a washboard manner, as a consequence of higher-order body resonances—to some 40 dB at $\omega \approx 10^4\ \mathrm{s}^{-1}$. These details are, however, not seen anymore in the total module loudness level.

The noise from the (four) wheels may also be computed by means of Eq. (30). In this case, the effective vibrating surface area amounts to $\Omega = \pi\mathsf{rw}$ per wheel, with $\mathsf{r} \approx 30\,\mathrm{cm}$ and $\mathsf{w} \approx 5\,\mathrm{cm}$. Further, one should replace ℓ in F by w. The wheels become audible only above $\omega \approx 10^3\,\mathrm{s}^{-1}$, and typically produce some 50 dB at $\omega \approx 10^4\,\mathrm{s}^{-1}$. Since this is still 10 dB less than the truck's loudness level at that frequency, the wheel contribution does not much affect $\mathsf{L}_{\mathrm{tot}}(\omega)$, which is given by Eq. (31) with $\Phi(\omega) = \Phi_{\mathrm{B}} + \Phi_{\mathrm{T}} + 4\Phi_{\mathrm{W}}$. For the threshold flux use was made of

$$\Phi_o(\omega) = \left[1 + (\omega_{\mathrm{s}}/\omega)^5\right]\Phi_o, \tag{32}$$

($\Phi_o = 10^{-12}\,\mathrm{Wm}^{-2}$) while the coefficient reads

$$\mathsf{d}(\omega) = 10^2/\log\left[\frac{(\omega_{\mathrm{s}}/\omega_{\mathrm{d}})^5}{1 + (\omega_{\mathrm{s}}/\omega)^5}\right]. \tag{33}$$

The result for the aluminum traction module ($\gamma^{1/2} = 164\,\mathrm{m}^2\,\mathrm{s}^{-1}$) is given in Fig. 5. The upper curve represents $\mathsf{L}_{\mathrm{tot|tr}}$ itself, the lower one gives $\Delta\mathsf{L}_{\mathrm{tot}}$. The free-running module thus yields $\mathsf{L}_{\mathrm{tot|fr}} = \mathsf{L}_{\mathrm{tot|tr}} + \Delta\mathsf{L}_{\mathrm{tot}}$, viz. shows an even more pronounced flexural resonance peak at $\omega_{\mathrm{m}} \approx 190\,\mathrm{s}^{-1}$, and exceeds 100 dB near $\omega \approx 550\ \mathrm{s}^{-1}$. The low-frequency resonance peak at ω_{m} is absent for the steel module ($\gamma^{1/2} = 450\,\mathrm{m}^2\ \mathrm{s}^{-1}$).

6 Final remarks

Modular low-floor lightrail systems are becoming the new worldwide standard in modern metropolitan railway developments. Examples can be found all over Europe (from Helsinki to Madrid, and from London to Athens), in Asia (e.g., in Istanbul), in Africa (e.g., in Tunis), in Japan (e.g., in Hiroshima), in Australia (e.g., in Melbourne and Sidney) and in the USA (e.g, in Boston, Los Angeles, San Diego, Houston, Phoenix, Portland, Minneapolis, and Seattle). It is a multibillion euro/dollar market, and the leading suppliers feel pressed to jump in and secure their share. Unfortunately, the new technology turned out to be more intricate than expected. Customers complaints concern inferior dynamical behavior of the wheels and trucks, substantially enhanced noise levels, and even cracks in the aluminium construction (see e.g., http:www.baluw.nl/combino). The present article is an attempt to clarify some of these design features from a theoretical physics point of view.

The mechanical model of modern lightrail modules defined in Eqs. (1)–(3) generalizes the standard suspension models of rigid vehicles to allow for the vibrational dynamics of a nonrigid coach construction (and for rubber wheel tyres). In this manner a comparison can be made between trams with steel or aluminium bodies.

The latter are important in view of recent developments in modular low-floor systems. The model is claimed to clarify certain novel dynamical instabilities in the wheel–rail contact, as well as related characteristic acoustical features. Special attention is also given to the problem of critical damping.

Inter alia, two pitfalls in the design of modern lightrail modules have been identified. Firstly, undercritical damping not only leads to unstable response characteristics (in particular for free-running modules), but also to significantly higher noise levels (typically 7 dB) over a wide frequency range. Secondly, a near coincidence of the truck resonance with the fundamental flexural body mode strongly enhances both the dynamical response (e.g., a factor four in the wheel spectrum) and the noise levels (up to an extra 10 dB at low but audible frequencies).

A Appendix: Critical damping

A.1 Exact analysis

Let us consider the rigid-body dynamics of Sect. 3, and investigate the exact conditions for critical damping. The three modes of this system follow from the zeroes of the denominator in $\eta_\omega = F_\omega Z_\omega / \Xi_\omega$, which using Eqs. (12)–(15) leads to $\Xi_\omega/\mu m M = \mathcal{R}_\omega + i\,\mathcal{I}_\omega$ with $\mathcal{R}_\omega = \sum_{n=0}^{3}(-1)^n \alpha_n \omega^{2n}$ (i.e., $\alpha_3 = 1$) and $\mathcal{I}_\omega = \sum_{n=0}^{2}(-1)^n \beta_n \omega^{2n+1}$, where

$$\begin{aligned}
\alpha_0 &= \frac{C_0C_1C_2}{\mu m M},\\
\alpha_1 &= \frac{C_0C_1}{\mu m}+\Big(1+\frac{m}{M}\Big)\frac{C_0C_2}{\mu m}+\Big(1+\frac{\mu+m}{M}\Big)\frac{C_1C_2}{\mu m}+\frac{C_0D_1D_2+C_1D_0D_2+C_2D_0D_1}{\mu m M},\\
\alpha_2 &= \frac{C_{01}}{\mu}+\frac{C_{12}}{m}+\frac{C_2}{M}+\frac{D_0D_{12}+D_1D_2}{\mu m}+\frac{D_{01}D_2}{\mu M}+\frac{D_1D_2}{mM},\\
\beta_0 &= \frac{D_0C_1C_2+D_1C_0C_2+D_2C_0C_1}{\mu m M},\\
\beta_1 &= \frac{D_0C_1+D_1C_0}{\mu m}+\Big(1+\frac{m}{M}\Big)\frac{D_0C_2+D_2C_0}{\mu m}+\Big(1+\frac{\mu+m}{M}\Big)\frac{D_1C_2+D_2C_1}{\mu m}+\frac{D_0D_1D_2}{\mu m M},\\
\beta_2 &= \frac{D_{01}}{\mu}+\frac{D_{12}}{m}+\frac{D_2}{M}.
\end{aligned} \tag{A.1}$$

For critical damping one should have $\Xi_\omega/\mu m M = -(\omega - i\Lambda_0)^2(\omega - i\Lambda_1)^2(\omega - i\Lambda_2)^2$, with real relaxation rates $\Lambda_j > 0$. Comparing this degenerate form with the general expression for Ξ_ω given above yields six conditions on the three rates, which are compatible only if the general coefficients satisfy three constraints, viz.

$$\alpha_1 = \frac{\beta_0^2}{4\alpha_0} + \beta_2\sqrt{\alpha_0},\ \alpha_2 = \frac{1}{4}\beta_2^2 + \frac{\beta_0}{\sqrt{\alpha_0}},\ \beta_1 = \frac{\beta_0\beta_2}{2\sqrt{\alpha_0}} + 2\sqrt{\alpha_0}. \tag{A.2}$$

Given C_0, C_1 and C_2, Eq. (A.2) yields the critical damping values for D_0, D_1 and D_2. Alternatively, e.g., given C_1, C_2 and D_0, one obtains the critical values for D_1, D_2 and C_0 (see Sect. 3.2). In principal, however, there exist several complex and real but negative valued solutions, while the relevant physical ones should all be positive. As already noted in Sect. 3.2, e.g., $D_1 > 0$ requires $\xi = \sqrt{MC_2/mC_1} < 1$. This turns out to be a minimum requirement sufficient only in the limit ($\mu/m \to 0, m/M \to 0$). Since the general case $\xi < \xi_c(\mu/m, m/M)$ is too involved for analytic treatment, let us consider the problem for $m/M \ll 1$ but with arbitrary μ/m.

A.2 Physical constraints

Rewriting Eq. (A.2) in terms of ξ, and $\nu = \sqrt{mC_1/\mu C_0}$, $\mathcal{X} = D_0/\sqrt{4mC_1}$, $\mathcal{Y} = D_1/\sqrt{4mC_1}$, $\mathcal{Z} = D_2/\sqrt{4mC_1}$, and then letting $M \to \infty$, at once yields $\mathcal{Z} = \xi$ and gives two equations that are now quadratic in $\mathcal{X}$ and $\mathcal{Y}$, and are solved by

$$\mathcal{X} = \frac{\big[1+2\hat\mu\nu-\hat\mu(1+\hat\mu)\nu^2\big]\nu\xi \pm \big[1-(1+\hat\mu)\nu\big]\sqrt{1-2\hat\mu\nu+\hat\mu(1+\hat\mu-4\xi^2)\nu^2}}{\big[1-2\hat\mu\nu+\hat\mu(1+\hat\mu)\nu^2\big]\nu} \tag{A.3}$$

and

$$\mathcal{Y} = \frac{\big[1-\hat\mu\nu(1+\nu)\big]\xi - (1-\hat\mu\nu)\nu\mathcal{X}}{(1+\hat\mu)\nu - 1}, \tag{A.4}$$

where $\hat\mu = \mu/m$. With $D_0 = 0$ (i.e., $\mathcal{X} = 0$), Eq. (A.4) immediately gives D_1 as

$$\mathcal{Y} = \frac{1-\hat\mu\nu(1+\nu)}{(1+\hat\mu)\nu - 1}\xi, \tag{A.5}$$

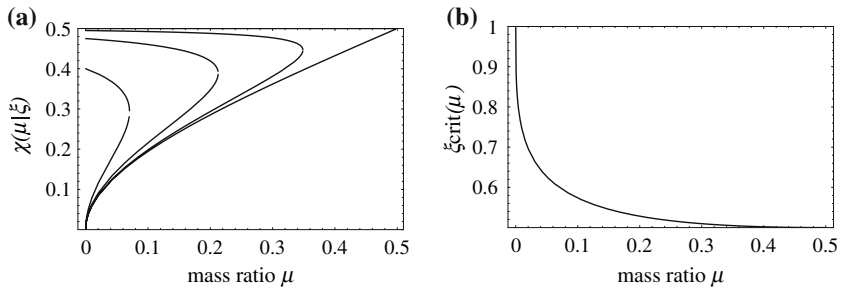

Fig. 6 Plot of **a** $\chi = 1/\nu(\hat{\mu})$ [$\nu = \sqrt{mC_1/\mu C_0}$] for several fixed values of $\xi = \sqrt{MC_2/mC_1}$ (from *left* to *right*: $\xi = 0.60; 0.525; 0.505; 0.50$), and **b** $\xi_c(\hat{\mu})$, showing the *borderline* between parameter regions where critical damping is mechanically possible ($\xi < \xi_c$) and where not

which (for $\hat{\mu} < \hat{\mu}_c$, see below) implies the physical constraint $\nu > 1/(1+\hat{\mu})$, while Eq. (A.3) boils down to finding the real positive zeroes (i.e., C_0) of the function

$$\mathcal{F}(\nu) = \left[\frac{1+2\hat{\mu}\nu-\hat{\mu}(1+\hat{\mu})\nu^2}{1-(1+\hat{\mu})\nu}\nu\xi\right]^2 - \left[1-2\hat{\mu}\nu+\hat{\mu}(1+\hat{\mu}-4\xi^2)\nu^2\right]. \tag{A.6}$$

For $\hat{\mu} = 0$, the polynomial $\mathcal{F}(\nu)$ becomes quadratic and the only solution satisfying $\nu > 1$ and $\xi > 0$ of Eq. (A.6) reads $\nu = 1/(1-\xi)$, with $\xi < 1$. However, from Eq. (A.3) one easily infers that if $\xi < \xi_c(\hat{\mu})$ there must be two real solutions (merging at $\nu = \nu_c$ if $\xi = \xi_c$). For $\hat{\mu} \to 0$, the second solution is found to be $\nu = \hat{\mu}^{-1/2}\sqrt{1/\xi^2 - 1}$. Noticing that these solutions tend to merge at $\nu \approx \hat{\mu}^{-1/3}$ for $1 - \zeta \approx \hat{\mu}^{1/3}$, suggests the proper scaling of the critical case in this limit. Indeed [ν_c and ξ_c follow from $\mathcal{F}'(\nu_c) = \mathcal{F}(\nu_c) = 0$], one finds $\nu_c = \hat{\mu}^{-1/3}\sum_n \nu_n \hat{\mu}^{n/3}$ with $\nu_0 = 1$, $\nu_1 = 1$, $\nu_2 = 0$, $\nu_3 = 1/3$, $\nu_4 = -1$, $\nu_5 = 0$, and so forth. Similarly, $\xi_c = \sum_n \xi_n \hat{\mu}^{n/3}$ with $\xi_0 = 1$, $\xi_1 = -3/2$, $\xi_2 = 15/8$, $\xi_3 = -43/16$, $\xi_4 = 667/128$, $\xi_5 = -2,213/256$, etc. Apart from the case $\hat{\mu} \ll 1$, another simple critical solution is immediately seen in Eq. (A.3), viz. $\nu = 2$ at $\xi = \hat{\mu} = 1/2$. In fact, $\nu = 2$ and $\xi = 1/2$ is a solution for all $\hat{\mu}$.

In fact, using e.g., Mathematica 5, one easily obtains exact general (for $M \to \infty$) expressions for $\xi(\nu, \hat{\mu})$ [or $\nu(\xi, \hat{\mu})$], and for $\xi_c(\hat{\mu})$ [and $\nu_c(\hat{\mu})$]. Figure 6a shows plots of $\nu(\hat{\mu}|\xi)$ for several fixed values of ξ, according to

$$\xi = \frac{1}{\nu}\frac{(1+\hat{\mu})\nu - 1}{\sqrt{1+4\hat{\mu}-2\hat{\mu}\nu+\hat{\mu}(1+\hat{\mu})\nu^2}}, \tag{A.7}$$

which clearly demonstrates the existence of two solutions for $\nu(\hat{\mu}|\xi)$ when $\xi < \xi_c$. The critical curve $\xi_c(\hat{\mu})$ is plotted in Fig. 6b using Eq. (A.7) with ν being replaced by

$$\nu_c = \frac{\hat{\mu} + \left[\hat{\mu}(1+2\hat{\mu})\right]^{2/3}}{\hat{\mu}(1+\hat{\mu})}. \tag{A.8}$$

The above analysis is strictly valid only up to $\hat{\mu} = \hat{\mu}_c$. First of all, for $\hat{\mu} > 4$ the physical constraint on Eq. (A.6) becomes either $1/(1+\hat{\mu}) < \nu < \nu_-$ or $\nu > \nu_+$, where $\nu_\pm = \frac{1}{2}(1 \pm \sqrt{1 - 4/\hat{\mu}})$. A new critical situation then occurs when $\nu_c(\hat{\mu} \to \hat{\mu}_c) = \nu_+$. This yields exact numerical expressions for $\hat{\mu}_c \approx 4.61$, $\nu_c(\hat{\mu}_c) \approx 0.68$, while for all $\hat{\mu} \geq \hat{\mu}_c$ one has $\xi_c = \sqrt{\nu_+}$, following from $\mathcal{F}(\nu_+) = 0$ only.

Note that the free-running module with $\hat{\mu} = 0.4$ and $\xi = 0.63$ does not fall in the physically allowed region below the curve $\xi_c(\hat{\mu})$ in Fig. 6b, while the traction unit with $\hat{\mu} = 0.24$ and $\xi = 0.45$ does.

References

1. van der Bijl, R.A.J.: Light rail and regional planning. Portland (OR): transport oriented development. Priemus, H., Kloosterman, R, Korthals Altes, W. (ed.) ICES, City & Infrastructure. Royal Van Gorcum, Assen (2003)
2. Hondius, H.: The development of low-floor trams. J. Adv. Transp. **27**, 1 (1993)
3. Hondius, H.: Stadverkehr, 49(11-12/2004)17–31; 50(1/2005)6–19; 50(10/ 2005)45–49
4. Goldstein, H.: Classical Mechanics. Addison-Wesley, Reading (1950)
5. Dekker, H.: Phys. Lett. **104**A, 72–76 (1984); **105**A 395–400 (1984)
6. Dekker, H. : Phys. Rev. A **31**, 1067–1076 (1985)
7. Landau, L.D., Lifshitz, E.M.: Theory of Elasticity, Course in Theoretical Physics, vol. 7. Pergamon Butterworth Heinemann, Oxford (1959/1986)
8. Pathria, R.K.: Statistical Mechanics. Pergamon, Oxford (1972)
9. Feynman, R.P.: The Feynman Lectures on Physics, Vol. I. Addison-Wesley, Reading Chap. 50 (1963/1988)
10. Bosworth, R.C.L.: Physics in Chemical Industry MacMillan, London (1950)
11. Bergeijk, W.A., Pierce, J.R., David, E.E. Jr.: Waves and the Ear. Anchor Books, New York (1960)
12. Landau, L.D., Lifshitz, E.M.: Fluid Mechanics, Course in Theoretical Physics, vol. 6. Pergamon Butterworth Heinemann, Oxford (1959/1987)
13. Beranek, L.L.: Acoustic Measurements. Wiley/Acoustical Society. America, New York (1949/1988)
14. Fletcher, H. : Rev. Mod. Phys. **12**, 47–65 (1940)
15. Levich, B.G.: Theoretical Physics, vol. 1. North-Holland, Amsterdam (1970)